JOURNAL OF Materials CHEMISTRY

Pyrrole- and polypyrrole-based liquid crystals

Yu Chen, Corrie T. Imrie and Karl S. Ryder*†

Department of Chemistry, University of Aberdeen, Meston Walk, Old Aberdeen, UK AB24 3UE

Received 17th November 2000, Accepted 23rd January 2001
First published as an Advance Article on the web 27th February 2001

In this paper we report one of the first examples of a soluble, fusible liquid crystalline polypyrrole. We describe the synthesis and characterisation of two pyrrole-based monomers substituted at the *N*-position with the mesogenic group 4-cyanobiphenyl. The mesogenic group is separated from the pyrrole moiety by an alkyl chain of either 3 or 11 methylene units length. We discuss the spectroscopic and thermotropic properties of these monomers and describe their oxidative polymerisation using electrochemical methods and separately using $FeCl_3$ and I_2 as chemical oxidants.

1 Introduction

Polypyrroles and polythiophenes have been the subjects of vigorous research interest because of the technological application of functionalised organic conductors. These applications have ranged from electroluminescent devices and FETs to enzyme-based sensors and artificial olfaction. However, these polymer materials are usually amorphous and often intractable solids. In our research we have sought routes to conducting polymer systems based on thiophene and/or pyrrole that both are soluble and exhibit ordered crystalline, or liquid crystal phases. Crystallinity or liquid crystallinity in these materials can not only provide an insight into the electronic conductivity, but is also expected to lead to new applications that exploit anisotropic behaviour associated with the discrete, orthogonal conductivity mechanisms along the conjugated strands of the polymer material and between adjacent strands. In addition to this, the anisotropic properties associated with the liquid crystal phases might be manipulated or switched through some external stimulus. Consequently, such materials are considered to be an important potential new feedstock for the plastic electronics industry. Although significant progress has been made in the synthesis of soluble/processable polymer systems by other research groups recently,[1] for example, by grafting long chain alkyl groups on to the pyrrole or thiophene ring, there remain very few examples of conducting polymer systems that exhibit liquid crystal phases.[2,3] Of particular interest, however, has been the development of pyrrole-based liquid crystalline systems[4–13] and here we describe the synthesis and characterisation of pyrrole-based monomers substituted at the *N*-position with the mesogenic group 4-cyanobiphenyl. We discuss the spectroscopic and thermotropic properties of these monomers and describe their oxidative polymerisation using electrochemical methods and separately using $FeCl_3$ and I_2 as chemical oxidants. The structures of the monomers, together with the acronyms we use to refer to them, are shown in Fig. 1.

It is generally accepted that large inter-chain spacing in polypyrroles and polythiophenes brought about by bulky substituents results in poor conductivity. However, it is also known that alkyl spacers are a key structural feature of a side group liquid crystal polymer in which their role is to decouple, to some extent, the orientational correlations of the mesogenic groups from those of the backbones. Thus, we have selected for study a system with both short and long alkyl spacers in order to elucidate these seemingly opposing tendencies. Although it is apparent that *N*-substituted materials exhibit lower conductivities than the analogous 3-substituted polypyrroles, we have chosen initially to study the former in order to obtain structurally regular materials. This will facilitate the interpretation of the thermal behaviour of the polymers.

2 Experimental

2.1 General methods

Commercial reagents were used without further purification. Solvents were purified and degassed according to standard procedures. ^1H and ^{13}C NMR data were obtained on Varian Unity Inova 400 MHz and Bruker AC-F 250 MHz spectrometers. FT-IR spectra were recorded using a Nicolet 205 FT-IR spectrometer, polymer film spectra were recorded *ex situ* using a specular reflectance accessory at an incident angle of 45°, or samples were prepared as KBr pressed films. In order to prevent spectral baseline distortion caused by conduction band effects the polymer samples were prepared in their fully reduced form. Mass spectra were recorded on a Finnigan Mass Lab Navigator. UV–Visible absorption spectra were recorded using a Perkin Elmer Lambda 9 spectrometer. The scanning electron microscopic measurements were performed on a JEOL JSM-5200 instrument under an accelerating voltage of 25 kV, and the specimens were fixed to aluminium stubs with Leit-C conducting cement. The thermal properties of the materials were determined by differential scanning calorimetry (DSC) using a Mettler Toledo 821 Differential Scanning Calorimeter at a heating/cooling rate of 10 °C min^{-1} under a constant flow of nitrogen and calibrated using indium. Phase identification

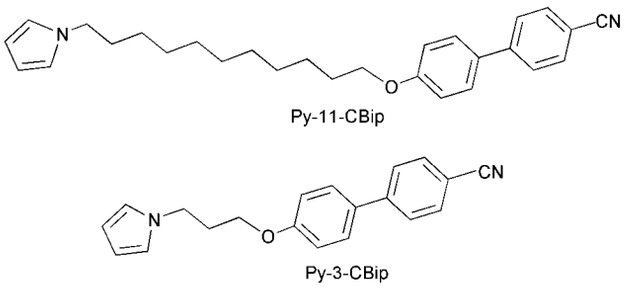

Fig. 1 Structures and acronyms of the pyrrole-based monomers and polymers.

†Permanent address: Department of Chemistry, De Montfort University, The Gateway, Leicester, UK LE1 9BH.

 DOI: 10.1039/b009237l

was performed by polarized light microscopy using an Olympus BH-2 optical microscope equipped with a Linkam THMS 600 heating stage and TMS91 control unit. The thermal stability of the polymers was assessed using a Mettler Toledo TGA/SDTA851e thermogravimetric analyser equipped with a Balzers Thermostar mass spectrometer. The heating rate was 10 °C min^{-1} and the atmosphere argon. The molecular weights of the polymers were measured by gel permeation chromatography (GPC) using a Knauer Instruments chromatograph equipped with two PL gel 10 μm mixed columns and controlled by Polymer Laboratories GPC SEC V5.1 Software. Chloroform was used as the eluent. A calibration curve was obtained using polystyrene standards.

All electrochemical procedures were carried out using an EG & G Princeton Applied Research potentiostat/galvanostat Model 263A driven by the M270 software package. A conventional three-electrode system was used in a single-compartment cell. A 0.05 M solution of $[NBu_4][BF_4]$ (recrystallised from CH_2Cl_2–diethyl ether) in dry acetonitrile (distilled over CaH) was used as a supporting electrolyte. The solutions were deoxygenated by bubbling dry argon for 5 minutes before each measurement and all experiments were carried out under an argon atmosphere. An AgCl/Ag electrode was used as a reference, which was held in a glass compartment with a Luggin capillary attached to the cell. A large platinum flag was used as a counter electrode. A gold foil (3.0 cm^2) was used as a working electrode for the electropolymerisation. For the cyclic voltammetry experiments, a platinum disc (4 mm) was used. The electrodes were cleaned by polishing with an aqueous slurry of 10 μm and 3 μm alumina before each measurement.

2.2 Synthesis

The *N*-[ω-(4-cyanobiphenyl-4′-yloxy)alkyl]pyrroles were prepared using the synthetic route shown in Scheme 1. The synthesis of the α-bromo-ω-(4-cyanobiphenyl-4′-yloxy)alkanes has been given elsewhere.[14]

2.2.1 Synthesis of *N*-[ω-(4-cyanobiphenyl-4′-yloxy)alkyl]pyrroles. The *N*-[ω-(4-cyanobiphenyl-4′-yloxy)alkyl]pyrroles were prepared using the procedure described by Ibison *et al.*[7] Thus, freshly distilled pyrrole (1.4 g, 0.02 mol) was added slowly to a dry diethyl ether solution (100 ml) of 18-crown-6 (0.53 g, 0.002 mol) and potassium *tert*-butoxide (2.24 g, 0.02 mol) in a 250 ml dry Schlenk round-bottom flask under an atmosphere of dry nitrogen. The mixture was stirred at room temperature for 15 minutes. The appropriate α-bromo-ω-(4-cyanobiphenyl-4′-yloxy)alkane (0.004 mol) was added slowly to the mixture, and the resulting solution was stirred for 24 hours. Water (50 ml) was added and the mixture extracted with diethyl ether (2 × 50 ml). The combined organics were washed with a saturated aqueous solution of NaCl (50 ml), water (2 × 50 ml) and then dried over anhydrous $MgSO_4$. The solvent was removed under reduced pressure and the crude product was purified by column chromatography (on silica gel, $CHCl_3$ as eluent), followed by recrystallisation from ethanol with hot filtration.

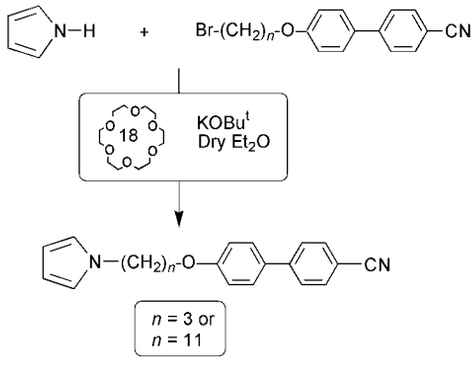

Scheme 1

N-[3-(4-Cyanobiphenyl-4′-yloxy)propyl]pyrrole, Py-3-CBip. White powder; yield: 44%; mp: 98 °C. FT-IR (KBr disk) ν/cm^{-1}: 3101 (C–H, Ar), 2942, 2877 (C–H, alkyl), 2220 (C≡), 1600, 1495 (C=C, Ar), 1245, 1176, 1072, (C–O–C, C–O–Ar), 821 (C–H out-of-plane, Ar), 736 (C–H out-of-plane, pyrrole). ^{1}H NMR ($CDCl_3$) δ (ppm): 7.66 (dd, $J=8$ Hz, 4H, aromatic), 7.52 (d, $J=8$ Hz, 2H, aromatic), 6.98 (d, $J=6$ Hz, 8 Hz, 2H, aromatic), 6.65 (t, $J=2$ Hz, 2H, pyrrole), 6.14 (t, $J=2$ Hz, 2H, pyrrole), 4.13 (t, $J=6$ Hz, 2H, NCH_2), 3.92 (t, $J=6$ Hz, 2H, OCH_2), 2.23 (quintet, $J=6$ Hz, 2H, $CH_2CH_2CH_2$).

N-[11-(4-Cyanobiphenyl-4′-yloxy)undecyl]pyrrole, Py-11-CBip. White powder; yield: 59%; mp: 86 °C. FT-IR: similar to Py-3-CBip. ^{1}H NMR ($CDCl_3$) δ (ppm): 7.66 (dd, $J=8$ Hz, 6 Hz, 4H, aromatic), 7.52 (d, $J=8$ Hz, 2H, aromatic), 6.98 (d, $J=8$ Hz, 2H, aromatic), 6.64 (t, $J=2$ Hz, 2H, pyrrole), 6.13 (t, $J=2$ Hz, 2H, pyrrole), 4.00 (t, $J=6$ Hz, 2H, NCH_2), 3.85 (t, $J=6$ Hz, 2H, OCH_2), 1.77 (quintet, $J=6$ Hz, 4H, NCH_2CH_2, OCH_2CH_2), 1.50–1.21 (m, 14H, $-(CH_2)_7-$).

2.3 Chemical polymerisation of Py-3-CBip and Py-11-CBip using iron(III) chloride

A solution of the monomer (0.001 mol) in freshly distilled chloroform (5 ml) was added to a suspension of anhydrous $FeCl_3$ (0.113 g, 0.0007 mol) in freshly distilled chloroform (50 ml) and the resulting mixture stirred at room temperature for 24 hours under nitrogen. The polymer in solution was precipitated by the addition of an excess of ethanol. The precipitate was boiled in absolute ethanol and the solvent decanted. This procedure was repeated until no unreacted monomer was detected in the solvent using thin layer chromatography. The black–brown residue was washed with chloroform, and the insoluble fraction dried under vacuum. A soluble fraction was obtained by removing the solvent and the solid was dried under vacuum.

Yield: poly(Py-3-CBip) 49%; poly(Py-11-CBip) 50%. Poly(Py-11-CBip): soluble fraction: solubility ($CHCl_3$) 4 mg ml^{-1}. ^{1}H NMR ($CDCl_3$) δ (ppm): 7.6 (broad, 4H, aromatic), 6.98 (broad, 4H, aromatic), 3.9 (broad 2H, NCH_2), 3.7 (broad, 2H, OCH_2), 1.7 (broad, 4H, NCH_2CH_2, OCH_2CH_2), 1.50–1.21 (m, 14H, $-(CH_2)_7-$). FT-IR (KBr disk) ν/cm^{-1} 2217 (C≡N).

2.4 Chemical polymerisation of Py-3-CBip and Py-11-CBip using iodine vapour

The monomer (0.001 mol) was spread over the bottom of a small beaker and exposed to saturated iodine vapour at room temperature for two days. The excess iodine was removed under vacuum at 60 °C for two hours and the polymer purified using the method described in Section 2.3. Poly(Py-11-CBip): brown powder; yield: 40%; solubility ($CHCl_3$) 4 mg ml^{-1}. Spectral analysis using FT-IR and ^{1}H NMR gave results indistinguishable from the polymers obtained using iron chloride.

2.5 Electrochemical polymerisation of Py-3-CBip and Py-11-CBip

The polymer film electrodes used for the cyclic voltammetric analysis were prepared on a platinum disc (4 mm) with 10 cycles of potential scan at 100 mV s^{-1} between 0 and 1.4 V (*vs.* AgCl/Ag) from the 0.01 M monomer, 0.05 M $[NBu_4][BF_4]$ acetonitrile solution, which were rinsed well with acetonitrile

then transferred to a monomer-free acetonitrile solution. The polymer films for reflectance FT-IR measurement were prepared on a 3 cm^2 gold foil electrode at a static potential of +1.4 V (*vs.* AgCl/Ag) from 0.01 M monomer, 0.05 M $[NBu_4][BF_4]$ acetonitrile solution. The chronoamperometric response was integrated to give a typical growth charge of 0.5 C cm^{-2}, which corresponds to an approximate film thickness of *ca.* 2 μm. The films on the gold flag electrode were washed with industrial methylated spirit (IMS) and acetone and then dried in air. The polymer films for characterisation using UV–Visible spectroscopy were prepared on a 2 cm^2 ITO glass electrode with 20 potential cycles at 100 mV s^{-1} between 0 and +1.4 V (*vs.* AgCl/Ag) from an acetonitrile solution containing 0.01 M monomer and 0.05 M $[NBu_4][BF_4]$. After 20 cycles a polymeric film had been deposited on the ITO electrode, which was washed with IMS and acetone then dried in air.

2.6 Conductivity measurements

The surface conductivities of electrochemically grown films were measured using a custom built dc linear four point probe apparatus with a Keithley Instruments high impedance electrometer as described in detail elsewhere.[15] For the infusible polymers prepared chemically, pellets (1 cm diameter) were prepared by pressing the sample (50 mg) under 5 ton for 30 min. The conductivities of these pellets were then evaluated using the four-point probe apparatus.

The conductivity of the fusible sample of poly(Py-11-CBip) was measured using a two-point probe arrangement. This was fabricated by depositing gold on to a glass substrate and this was mounted on a Linkam THMS 600 heating stage, allowing conductivity to be measured as a function of temperature. The area between the probes was 11×10 μm^2. The resistance, R, of the sample was measured using a Keithley Instruments high impedance electrometer and the surface conductivity, σ, calculated using the relationship, $\sigma = (RA/l)^{-1}$ where A is the area of the sample measured and l the sample length (11 μm).

3 Results and discussion

3.1 Electrochemical properties of Py-3-CBip and Py-11-CBip

Cyclic voltammetry in 0.05 M $[NBu_4][BF_4]$ MeCN solution of both monomer species revealed irreversible anodic oxidation leading to polymer formation. A typical multi-sweep voltammogram of Py-11-CBip is presented in Fig. 2. The first voltammogram of this series clearly shows the anodic current cross-over feature associated with polymer nucleation at the electrode surface. Oxidation of the cyanobiphenyl group was not observed under these experimental conditions prior to the anodic potential limit of the electrolyte system. Subsequent scans all show the gradual increase of the quasi-reversible redox process associated with the doping/dedoping reaction of the growing polymer film. Similar behaviour was also observed for Py-3-CBip. Polymerisation of both monomers was facile under these conditions and also using potentiostatic/chronoamperometric or galvanostatic techniques. Free-standing films were obtained for analysis using scanning electron microscopy and FT-IR spectroscopy and for conductivity measurements . The absorbance/reflectance mode FT-IR spectrum of a poly(Py-11-CBip) film is shown in, Fig. 3a, alongside that of the monomer species Fig. 3b (KBr disk) for comparison. The ν(CN) stretch is clearly visible in the spectra of both the polymer and the monomer at 2223 cm^{-1}, confirming the presence of the mesogenic unit in the polymer material. Additionally the absorbance at 723 cm^{-1} in the spectrum of the monomer (Fig. 3b), attributed to the α-(C–H) bending mode of the pyrrole ring. is absent in the polymer indicating α–α coupling of the pyrrole units in the polymer material.

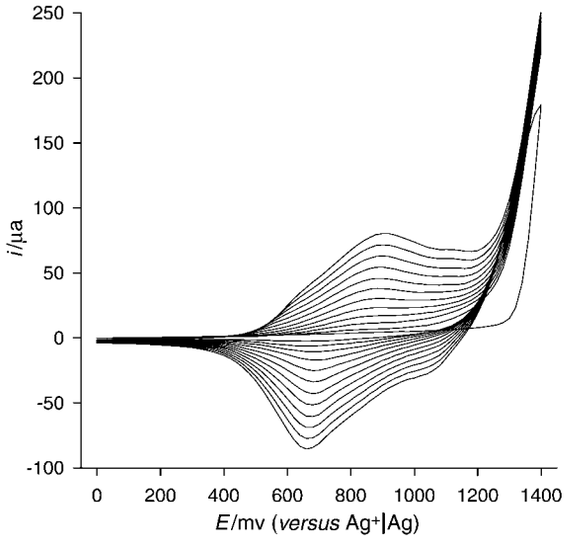

Fig. 2 Polymerisation of Py-11-CBip using repetitive scan cyclic voltammetry. This set of CVs was recorded at a Pt disk electrode (diameter = 4 mm) in 0.05 M $[NBu_4][BF_4]$–MeCN electrolyte, 10 mM Py-11-CBip, using a potential scan rate of 100 mV s^{-1}.

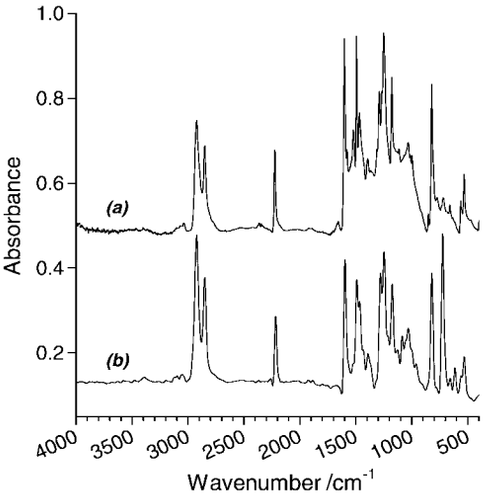

Fig. 3 (a) Absorbance/reflectance FT-IR spectrum of poly(Py-11-CBip) produced using the repetitive CV method (Fig. 2). The polymer (approximate thickness 1–2 μm) was adhered to an Au-coated glass slide. (b) Absorbance FT-IR spectrum of Py-11-CBip (monomer) as a KBr disk. Both spectra were acquired at a resolution of 4 cm^{-1}.

Whilst the peak anodic potentials for the irreversible oxidation reactions of the two monomer species are similar (Table 1), the rate of growth of polymer was found to be 60–70% slower for Py-11-CBip than for the shorter homologue.‡ This is consistent with the steric constraints imposed on the larger molecule and, presumably, is also a function of a smaller diffusion coefficient.

Subsequent to polymer film formation, the coated electrode assembly was then removed from solution and examined by cyclic voltammetry in a fresh, monomer-free electrolyte solution. These electrode assemblies showed the quasi-reversible redox process associated with the conducting polymer film. Relevant peak potential and spectral data are presented in Table 1. The magnitude of the anodic peak current for these processes showed a linear dependence on potential scan rate confirming that the redox reaction was confined to the electrode surface (Fig. 4).

‡The rate of polymer growth was determined from the total charge passed in a chronoamperometric experiment after a fixed period of time, typically 2–5 min, under diffusion-controlled conditions.

Table 1

Monomers		Polymers		
	E_{pa}/V (*vs.* AgCl/Ag)	$E_{pa}:E_{pc}$/V (*vs.* AgCl/Ag)	UV–Vis λ_{max}/nm	Conductivity σ/S cm^{-1}
Py-3-CBip	1.40	0.80 : 0.54	322	7×10^{-4}
Py-11-CBip	1.51	0.93 : 0.75	316	8×10^{-5}

Polymer films, of both monomer species, grown on indium tin oxide coated (ITO) glass electrodes were examined by UV–Visible spectroscopy and both films showed absorbances typical for *N*-substituted polypyrroles (Table 1). The λ_{max} values of 322 and 316 nm for poly(Py-3-CBip) and poly(Py-11-CBip) respectively, compared to unsubstituted pyrrole, typically $\lambda_{max}=220$ nm, are indicative of a large HOMO–LUMO "band" gap. This is consistent with the poor surface conductivities of these materials determined here from free-standing samples of poly(Py-3-CBip) and poly(Py-11-CBip) (see Table 1). The latter point is a well known and unfortunate consequence of pyrrole substitution at the *N*-position.

Polymer films of both species showed good stability under redox cycling. In a typical experiment a polymer coated electrode was cycled thirty times from 0 to +1200 mV (at 100 mV s^{-1}). Whilst an initial 10% decrease of peak current was observed following the first anodic scan the remaining twenty nine scans showed only very minor deviations in charge–discharge behaviour. This observation was confirmed by comparing the voltammograms of polymer films before and after storage in air for one month. No significant changes were revealed. The stability of these films, manifest in their electrochemical characteristics, is also confirmed by their thermal properties, discussed later.

Somewhat disappointingly, the materials obtained from electrochemical polymerisation of the two species described here were all infusible and insoluble. The solid, free-standing films showed no evidence of thermally induced phase transitions before their decomposition temperatures. This is consistent with the observations of other groups investigating similar systems and may be the consequence of a high level of defect formation or cross-linking in the polymer matrix. Conductivity of the electrochemically produced materials was low at 10^{-4}–10^{-5} S cm^{-1}. Consequently we proceeded to investigate the properties of polymer materials derived from chemical oxidants including $FeCl_3$ and molecular iodine.

3.2 Thermal behaviour of Py-3-CBip and Py-11-CBip

Liquid crystalline behaviour was not observed for Py-3-CBip, which melted directly into the isotropic phase at 98 °C. Py-11-CBip also melted directly into the isotropic phase, although at a lower temperature, 86 °C, and in addition, exhibited a monotropic nematic phase. The nematic–isotropic transition temperature, T_{NI}, is 56 °C and the phase was identified on the basis of a characteristic schlieren optical texture when viewed through the polarised light microscope. Unfortunately, the rapid crystallisation of the nematic phase prevented any further characterisation. The isotropic phase of Py-11-CBip could be supercooled to 45 °C prior to the onset of crystallisation.

The only other homologue belonging to this series to be reported in the literature is the hexyl member, *i.e.* Py-6-CBip,[7,8,10] which melts at 88 °C and exhibits a T_{NI} at 14 °C. The significantly lower T_{NI} exhibited by Py-6-CBip, compared to that shown by Py-11-CBip, reflects the difference in the average molecular shape of the two compounds, which is controlled, to a large extent, by the parity of the alkyl chain (see schematic representations in Fig. 5). Thus, for Py-11-CBip the symmetry axes of the mesogenic and pyrrole units are coparallel, whereas for Py-6-CBip they are inclined at an angle. The structure of Py-11-CBip is more compatible, therefore, with the molecular

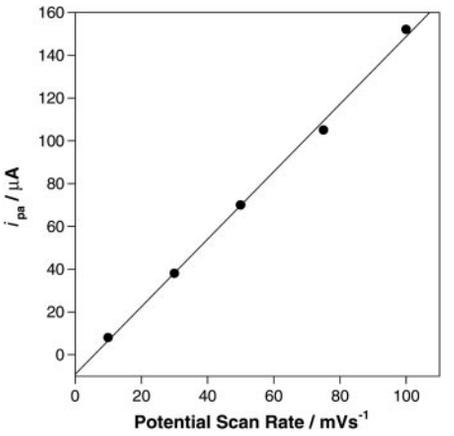

Fig. 4 Potential scan rate dependence of peak anodic current, i_{pa}, for a Pt disk electrode coated with poly(Py-3-CBip).

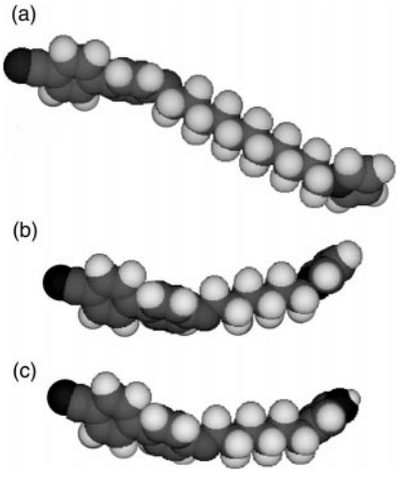

Fig. 5 Schematic representations of the molecular shapes of (a) Py-11-CBip and (b) Py-6-CBip with the spacer in the all-*trans* conformation. Also shown is (c) the analogous structure to (b) but based on 3-substitution of the pyrrole ring.

organisation found in the nematic phase and this greater compatibility results in the higher T_{NI}. Similar arguments have been offered to rationalise the behaviour of liquid crystal dimers in which two mesogenic units are separated by a flexible spacer.[16,17] We note, however, that such an argument neglects the flexibility of the alkyl chain and a more realistic interpretation would include a wider range of conformations and not solely the all-*trans* conformation.[17] The lower clearing temperature shown by Py-3-CBip compared with Py-11-CBip is in accord with the very general observation that for homologous liquid crystal series having clearing temperatures lower than *ca.* 100 °C, increasing the length of an alkyl chain promotes liquid crystalline behaviour.[18] This reflects the role played by the alkyl chain in enhancing the shape anisotropy of the molecule.

It is evident from the literature that attachment of the liquid crystal groups at the 3-position rather than the *N*-site of the pyrrole ring results in higher clearing temperatures.[4,8,9] No explanation of this observation has been offered and it is not immediately apparent that such behaviour fits within the framework proposed to rationalise the relative T_{NI}s of Py-11-CBip and Py-6-CBip. If we again consider the average molecular shapes, as represented by the all-*trans* conformation, then the shapes of the *N*-substituted and 3-substituted pyrroles are essentially identical, see Fig. 5. The most probable explanation for this difference in thermal behaviour considers the possibility of hydrogen bond formation for the 3-substituted materials, with the pyrrole unit acting as the

hydrogen bond donor and the nitrile group as the hydrogen bond acceptor. This may lead to the formation of a supramolecular polymeric system[19] with an enhancement in the clearing temperature. Such an arrangement is clearly not possible for the *N*-substituted derivative for which there is no hydrogen bond donor.

3.3 Polymer synthesis and characterisation

Both monomers underwent chemical polymerisation using either anhydrous $FeCl_3$ or I_2 as the oxidant. In each case two fractions were obtained, one soluble in chloroform and the other insoluble. Only in the synthesis of poly(Py-11-CBip) was sufficient soluble material isolated for characterisation purposes. We assume that the insoluble fraction either consists of considerably higher molecular weight polymer or is cross-linked through the 3-positions on the pyrrole units.

The number average molecular weight of the soluble fraction of poly(Py-11-CBip) obtained using anhydrous $FeCl_3$ as the oxidant was estimated using GPC as 17600 g mol^{-1} with an associated polydispersity of 1.7; this corresponds to a degree of polymerisation of *ca.* 42. The soluble polymer obtained using I_2 as the oxidant had a lower number average molecular weight, 3500 g mol^{-1}, a polydispersity of 1.9 and a degree of polymerisation of *ca.* 8. This reduction in molecular weight is presumably a consequence of the lower redox potential of I_2. In addition, solid phase polymerisation does not facilitate the long-range molecular rearrangements and diffusion necessary for the formation of high molecular weight materials. The UV–Visible spectrum of poly(Py-11-CBip) measured in chloroform contains two broad bands at *ca.* 290–300 and 360–370 nm. The former band is associated with the π–π* transition of the biphenyl moiety and is present in the spectrum of both the monomer and the polymer, while the latter band is assigned to the π–π* transition of the polypyrrole-based backbone. The breadth of this band implies a range of differing conjugation lengths, a view consistent with the relatively high polydispersity measured using GPC.

3.3.1 Thermal behaviour of poly(Py-3-CBip) and poly(Py-11-CBip). The insoluble fractions prepared chemically of both monomers, in common with the electrochemically prepared samples, were infusible, decomposing prior to melting. By contrast, the DSC trace obtained on reheating the soluble fractions of poly(Py-11-CBip) contained a step-change in the heat capacity at 92 °C and a broad, weak endotherm centred at 154 °C. The latter transition was identified on the basis of the optical texture observed through a polarised light microscope. In preparation for this identification, the polymer was heated to approximately 10 °C above the clearing temperature and then cooled at 0.2 °C min^{-1} into the mesophase. At the transition, a poorly defined, focal conic fan texture developed (Fig. 6). This texture is not sufficiently well-defined to permit an unambiguous phase identification but strongly suggests a smectic A phase. Thus, the broad endotherm in the DSC trace is assigned as a smectic A–isotropic transition. The breadth of the transition reflects both the relatively high polydispersity and possibly, structural inhomogeneities. The optical texture did not change on cooling to room temperature and hence, the lower temperature transition is assigned as a glass transition.

The conductivity of the soluble/fusible fractions of poly(Py-11-CBip) was determined both for the amorphous material and for the glassy solid formed on cooling from the smectic liquid crystal phase. The conductivities were low and consistent with the values obtained for the electrochemically prepared films, with $\sigma < 10^{-5}$ S cm^{-1}. This is most probably due to the very large steric bulk of the substituent at the *N*-position that acts both to separate the pyrrole chains, slowing the rate of electron hopping, and to reduce conjugation length of the polymer through chain twisting. On heating to the molten isotropic phase (175 °C), however, the conductivity of poly(Py-11-CBip) increased to 6.6×10^{-5} S cm^{-1}. This latter observation is most probably the consequence of more rapid chain and segmental motion of the polymer strands that acts to increase the rate of inter-chain electron hopping.

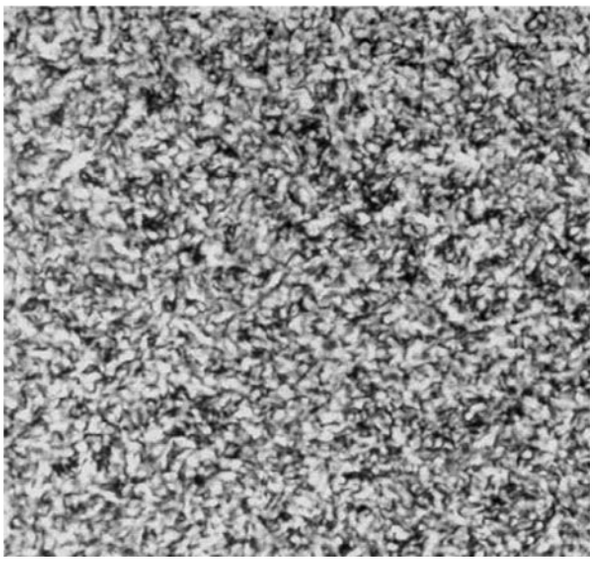

Fig. 6 Optical texture exhibited by the soluble fraction of poly(Py-11-CBip).

Cyanobiphenyl has become the benchmark in comparisons of the effects of backbone flexibility on the transitional properties of side group liquid crystal polymers (SGLCP).[20,21] Such a comparison reveals that for a given combination of alkyl spacer and mesogenic group, increasing backbone flexibility generally increases the clearing temperature while decreasing the glass transition temperature. Thus, a polystyrene-based SGLCP exhibits a higher glass transition temperature, but a lower clearing temperature, than the analogous polysiloxane-based SGLCP. However, poly(Py-11-CBip) does not fit into this pattern of behaviour, and exhibits a high glass transition temperature combined with a high clearing temperature, comparable to those of poly(vinyl ether)- and polysiloxane-based materials. Similarly surprising behaviour has been reported recently for poly(*p*-phenylene)-based SGLCPs.[22] For example, the undecyl homologue of this series exhibits a glass transition at 43 °C and a nematic–isotropic transition at 158 °C. There are two possible explanations for this behaviour. If we first consider conventional SGLCPs then it is interactions between the mesogenic side groups that drive the formation of the liquid crystal phase, while the liquid crystal field distorts the backbone from a random coil conformation into an ellipsoid. This field is thought to be sufficiently strong to confine a flexible backbone to lie between the smectic layers forming a microphase separated morphology. For more rigid backbones such an arrangement is not achieved and instead the backbone passes through the liquid crystal domains. In doing so the backbone is forced to adopt more extended conformations. At the clearing transition, therefore, there will be a greater change in the conformational distribution of a rigid backbone than for a flexible backbone. Hence, the more rigid backbones exhibit lower clearing temperatures. Extrapolating this argument, it has been assumed that the maximum possible clearing temperature for an SGLCP would be achieved in the limiting condition of an infinitely flexible backbone. If we now consider, however, a wholly rigid backbone then this will also be confined to lie between the layers allowing maximum interactions between the side groups and hence, high clearing temperatures. Thus, we predict that increasing the rigidity of the backbone in a conventional SGLCP initially causes a

decrease in the clearing temperature but as rigidity continues to increase the clearing temperature will pass through a minimum and then increase. Such behaviour has yet to be seen experimentally.

An alternative explanation of the anomalously high clearing temperatures seen for the polypyrrole- and poly(*p*-phenylene)-based SGLCPs considers the inherent liquid crystallinity of these backbones. The clearing temperatures of polypyrrole and poly(*p*-phenylene) are undoubtedly very high, but in practice decomposition precludes the observation of liquid crystalline behaviour. The addition of bulky side groups will reduce the glass transition and clearing temperatures and at some critical concentration these will fall to below the decomposition temperature of the polymer. Thus, it is possible that the side groups are acting, in effect, as plasticisers by reducing the interactions between the backbones and so revealing liquid crystalline behaviour.

Both these possible explanations are supported by the similarity in clearing temperatures between the polypyrrole- and poly(*p*-phenylene)-based SGLCPs. This suggests that poly(Py-11-CBip) has a linear structure without an appreciable number of structural defects. It is interesting to note, however, that the glass transition temperature of the polypyrrole-based SGLCP is considerably higher. This may indicate that the synthesis of the poly(*p*-phenylene)-based SGLCPs gave a regio-irregular distribution of the side groups[22] and this would act to reduce the glass transition temperature.

3.3.2 Thermal stability of poly(Py-11-CBip). The thermal stabilities of poly(Py-11-CBip) prepared electrochemically and the soluble and insoluble fractions obtained by chemical means were assessed using thermogravimetric analysis. Each sample was stable to temperatures in excess of 300 °C whereas polypyrrole prepared either chemically or electrochemically exhibits 10% weight loss at 300 °C.[23,24] By comparison, 10% weight loss occurred at 341 °C for the chloroform soluble sample, 385 °C for the insoluble chemically prepared sample and 387 °C for the electrochemically prepared sample. The similarity in thermal stability of the two insoluble samples strongly suggests similar structures with essentially the same degree of cross-linking. This view is supported by the FT-IR spectra of these polymers, which are identical. The lower decomposition temperature for the soluble sample is in agreement with the view that this fraction has a lower molecular weight and/or is cross-linked to a much lesser extent.

4 Conclusions

Here we have investigated the thermal, spectroscopic and electrochemical properties of polymers derived from two pyrrole monomers substituted at the *N*-position with a cyanobiphenyl mesogenic group. We have shown that polymerisation of these compounds using electrochemical techniques leads to insoluble and infusible materials that show no liquid crystal phases. On the contrary, poly(Py-11-CBip) produced using homogeneous chemical oxidants produced a soluble and fusible polymer with a stable mesophase whose optical texture was consistent with a smectic A structure. The poor conductivity of all the materials discussed here is probably a consequence of the *N*-substitution and of the steric bulk of the substituent. Nevertheless the latter clearly has an important role in determining the overall stability and order of the mesophase. The soluble and fusible nature of poly(Py-11-CBip) and the clearing temperature indicate that this is a linear polymer with relatively low defect population or cross-linking.

References

1 R. D. McColough and P. C. Ewbank, in *Handbook of Conducting Polymers*, 2nd edn., ed. T. A. Skotheim, R. L. Elsenbaumer, and J. R. Reynolds, Marcel Dekker, New York, 1998.
2 B. Faye, M. Mauzac and J. P. Parneix, *Synth. Met.*, 1999, **99**(2), 115; A. G. Macdiarmid, *Synth. Met.*, 1997, **84**, 27; Y. C. Kim, M. W. Kim, S. S. Pak and C. Y. Kim, *Mol. Cryst. Liq. Cryst. Sci. Technol., Sect. A*, 1998, **319**, 183.
3 S. Abe, M. Kijima and H. Shirakawa, *J. Mater. Chem.*, 2000, **10**, 1509.
4 P. J. Langley, F. J. Davis and G. R. Mitchell, *Mol. Cryst. Liq. Cryst.*, 1993, **234**, 765.
5 D. Melamed, C. Nuckols and M. A. Fox, *Tetrahedron Lett.*, 1994, **35**, 8329.
6 F. Vicentini, J. Barrouillet, R. Laversanne, M. Mauzac, F. Bibonne and J. P. Parneix, *Liq. Cryst.*, 1995, **19**, 235.
7 P. Ibison, P. J. S. Foot and J. W. Brown, *Synth. Met.*, 1996, **76**, 297.
8 H. Hasegawa, M. Kijima and H. Shirakawa, *Synth. Met.*, 1997, **84**, 177.
9 P. J. Langley, F. J. Davis and G. R. Mitchell, *J. Chem. Soc., Perkin Trans. 2*, 1997, 2229.
10 M. Kijima, H. Hasegawa and H. Shirakawa, *J. Polym. Sci., Part A: Polym. Chem.*, 1998, **36**, 2691.
11 C. Jego, E. Dupart, P. A. Albauy and C. Mingotaud, *Thin Solid Films*, 1998, **329**, 1.
12 B. Faye, M. Mauzac and J. P. Parneix, *Synth. Met.*, 1999, **99**, 115.
13 M. Kijima, S. Abe and H. Shirakawa, *Synth. Met.*, 1999, **101**, 61.
14 G. S. Attard, C. T. Imrie and F. E. Karasz, *Chem. Mater.*, 1992, **4**, 1246.
15 Y. Chen, C. T. Imrie, J. M. Cooper, A. Glidle, D. G. Morris and K. S. Ryder, *Polym. Int.*, 1998, **47**, 43.
16 C. T. Imrie, *Struct. Bonding (Berlin)*, 1999, **95**, 149.
17 C. T. Imrie and G. R. Luckhurst, in *Handbook of Liquid Crystals*, vol. 2B, ed. D. Demus, J. Goodby, G. W. Gray, H.-W. Spiess and V. Vill, Wiley-VCH, Weinheim, 1998, ch. 10, pp. 801–834.
18 C. T. Imrie and L. Taylor, *Liq. Cryst.*, 1989, **6**, 1.
19 C. T. Imrie, *Trends Polym. Sci.*, 1995, **3**, 22.
20 C. T. Imrie, F. E. Karasz and G. S. Attard, *Macromolecules*, 1993, **26**, 3803.
21 A. A. Craig and C. T. Imrie, *Macromolecules*, 1995, **28**, 3617.
22 V. Percec, A. D. Asandei, D. H. Hill and C. Crawford, *Macromolecules*, 1999, **32**, 2597.
23 J. A. Walker, L. F. Warren and E. F. Witucki, *J. Polym. Sci., Part A: Polym. Chem.*, 1988, **26**, 1285.
24 A. F. Diaz and K. K. Kanazawa, in *Extended Linear Chain Compounds*, vol. 3, ed. J. S. Miller, Plenum Press, New York, 1983, p. 426.